

We are IntechOpen, the world's leading publisher of Open Access books Built by scientists, for scientists

6,900

Open access books available

186,000

International authors and editors

200M

Downloads

Our authors are among the

154

Countries delivered to

TOP 1%

most cited scientists

12.2%

Contributors from top 500 universities



WEB OF SCIENCE™

Selection of our books indexed in the Book Citation Index
in Web of Science™ Core Collection (BKCI)

Interested in publishing with us?
Contact book.department@intechopen.com

Numbers displayed above are based on latest data collected.
For more information visit www.intechopen.com



Damage Identification and Assessment Using Lamb Wave Propagation Parameters and Material Damping in FRP Composite Laminates

Beera Satish Ben and Beera Avinash Ben

Abstract

A methodology for identify damage in the fiber reinforced polymer (FRP) composite has been proposed in this article. The Lamb wave dispersion theory was used to find the fitted peak frequency and loss less finite element model was used to find the modal frequencies in the composite laminates. The change in modal parameters with respect to undamaged and damaged specimen has been considered for the structural diagnosis. The combined finite element and Lamb wave method has been used to obtain damping parameters. The damping capacity was calculated at higher frequency and smaller amplitudes by using hybrid method. The Lamb waves were generated using ultrasonic pulse generator setup. The proposed method was implemented on FRP laminates (CFRP and GFRP) and the results were compared with bandwidth method.

Keywords: carbon fibers, Lamb wave, glass fibers, vibration, damping, acoustic emission

1. Introduction

Composite materials with advanced properties like, high specific strength and fatigue resistance are being used for many components of aircraft structures in recent era. However, they have high chances of failure when they are subjected to low velocity-impact, which could lead to barely visible impact damage (BVID). BVID are considered to be internal defects which can lead to catastrophic accidents in service. Damage is defined as the changes introduced into a system that leads to affect adversely to its current or future performance. Damage assessment techniques in the structural dynamics have been divided into three categories such as linear, non-linear and transient vibrational measurements. The change in modal parameters such as natural frequencies and material damping can be considered as the prevalent damage detection methods in structural assessment procedure. The existing damage in a structure, leads to the reduction in stiffness and consequently decreasing of the natural frequencies of the system.

According to Doebling et al. [1] damage detection by using vibration measurement in elastomers has been first reported by Lifshitz and Rotem [2]. They used the changes in the dynamic moduli and change in the natural frequencies to detect damage.

Many researchers identified crack depth and location from the dependency of the first two structural Eigen frequencies and presented contour graph. The superposed contour of the frequencies variations between the undamaged and damaged structures is used to identification the damage. The intersection point of superposed contour allows identifying both the crack depth and location [3].

According to Gillich and Praisach [4] the change in damping and the friction between crack surfaces lead to dissipative effects. The advantages of using changes in damping is that the cracks allows changes in natural frequencies due to uncertainties and cause important changes in the damping factor allowing damage detection.

Kyriazoglou and Guild [5] predicted damping parameters of GFRP and CFRP laminates by using finite element model. Most of the damping related calculations and experiments were carried out by Berthelot and Sefrani [6–8] for various composites using Ritz Method. They have performed damping analysis of composite plate and structures by using this method [9–11].

Chen and Gibson [12] have studied damping mechanisms in composites which involves a variety of energy dissipation mechanisms. The vibrational parameters such as frequency and amplitude in fiber-reinforced polymers that depend on energy dissipation mechanisms are studied with nondestructive evaluation.

Many researchers have used nondestructive evaluation (NDE) techniques to characterize the fiber-reinforced composites [13, 14]. Energy dissipation theory has been used for measuring damping capacity based on vibration damping method.

Damping measurement techniques often deal with natural frequency or resonant frequency of a system. The experimental setup to find the vibration is categorized as free vibration (or free decay) and forced vibration. Free-free beam technique and the piezoelectric ultrasonic composite oscillator technique (PUCOT) are forced vibration techniques. Dynamic mechanical analysis (DMA) uses these techniques to find damping characteristics of the material. However, the instrument is relatively expensive and it cannot be operated at higher frequency and low amplitudes where more information from the tested materials can be obtained [15].

Guan and Gibson [16] have developed micromechanical models for damping in woven fabric-reinforced polymer matrix composites. Where as many other researchers has published results for continuous FRP composites that show damping characteristics of composite material come from microplastic or viscoelastic phenomena associated with the matrix and slippage at the interface between the matrix and the reinforcement [17, 18].

The article presents the methodology to find viscous damping, which is the dominant mechanism in FRP composites vibrating at small amplitudes. A hybrid method employing combined finite element and frequency response has been developed to measure the damping properties of composite material.

2. Experimental setup

2.1 Ultrasonic pulse generator

In this work the specimens are carbon fiber/epoxy (CFRP) and glass fiber/epoxy (GFRP) laminates. The laminate contains woven fiber with 12 plays with average epoxy layer thickness of 0.2 mm. **Figure 1** shows the specimen with the dimensions

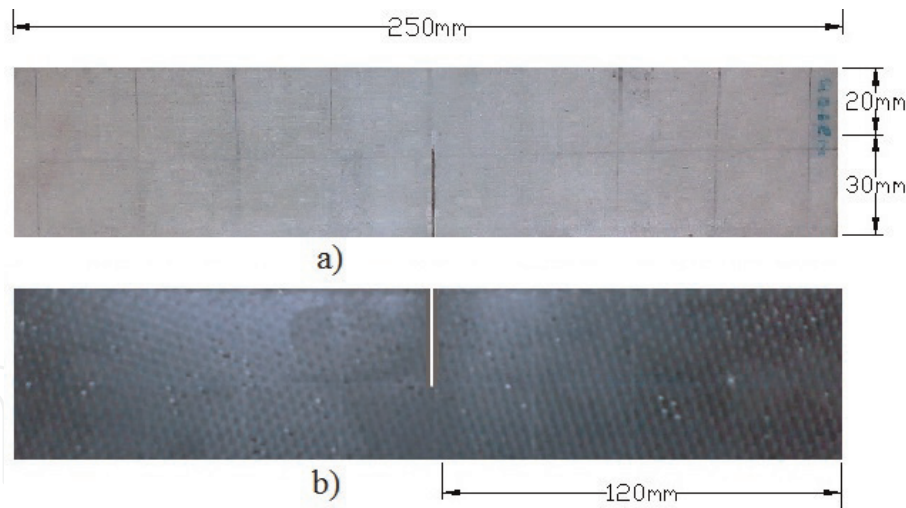


Figure 1.
Damaged specimen: (a) GFRP and (b) CFRP.



Figure 2.
Experimental setup.

250 × 50 × 2 mm in damaged state where a cut (30 × 2 × 2 mm) at a distance 120 mm away from free end has been introduced.

Figure 2 shows an experimental setup to develop Lamb waves using ultrasonic equipment NDT™ EPOCH 4PLUS. The specimen is supported as cantilever; pitch-catch radio frequency (RF) test method was used. Dual-element transducers (DIC-0408) where one element transmits and the other element receives the burst of acoustic waves generated in the specimen. 1 kHz to 4 MHz frequency range transducers was used and they were placed 80 mm apart from each other. Honey glycerine couplant made by Panametrics has been used to couple the two sensors on to the test specimen. The couplant helps to transmit a normal incident shear wave to propagate across the test piece between the transducer tips. Scanview plus™ software was used to acquire and process the data obtained from the test specimens [19, 20].

2.2 Generation of optimal Lamb wave

Acoustic impedance of the material plays important role in deciding the selection of transducer frequency, low impedance require lower frequency transducers. The materials such as carbon fiber or glass fiber have low impedance thus low frequency transducers will be used to generate Lamb waves. Whereas metal skin layers have high impedance therefore higher frequencies transducers are used for thinner and metallic layers.

The Panametrics-NDT™ EPOCH 4 PLUS is used to generate acoustic waves and the device is equipped with four channels. Optimal Lamb wave propagation parameters were arrived through calibration of the device using editable parameters as shown in **Table 1**.

The parameters have been varied one by one and arrived to a conclusion of optimal driving frequency for different specimens. **Figure 3** shows the optimal driving frequency of different materials calibrated through ultrasonic pulse generator test setup. With the help fitted peak value and percentage amplitude at constant gain 55 (db) Lamb waves generation frequency is identified for different materials. **Figure 4** shows the histogram representation of % amplitude of the waveform with a bin range of 0–820 kHz of pulser [21, 22]. The most effective range of frequencies to generate Lamb waves is 140–420 kHz. The frequency range to generate Lamb waves for GFRP is 170–190 kHz where as it is 260–280 kHz for CFRP and for Aluminum (Al) it is 360–380 kHz.

2.3 Material properties

The Young’s modulus for the specimens is calculated from Eq. 1, the calibrated experimental setup is used to generate Acoustic Emission (AE) on to the test specimen. AE velocities travelling in the material are determining from the instrument EPOCH 4 PLUS [22, 23].

Editable parameters							
Pulser	Mode	Receiver	Gain	Device	Unit	Waveform	Rang
	Energy		Broad band		Angle		Rectification
	Wave Type		Low pass		Thickness		Offset
	Frequency		High pass				
			By pass				

Table 1.
EPOCH 4 PLUS parameters.

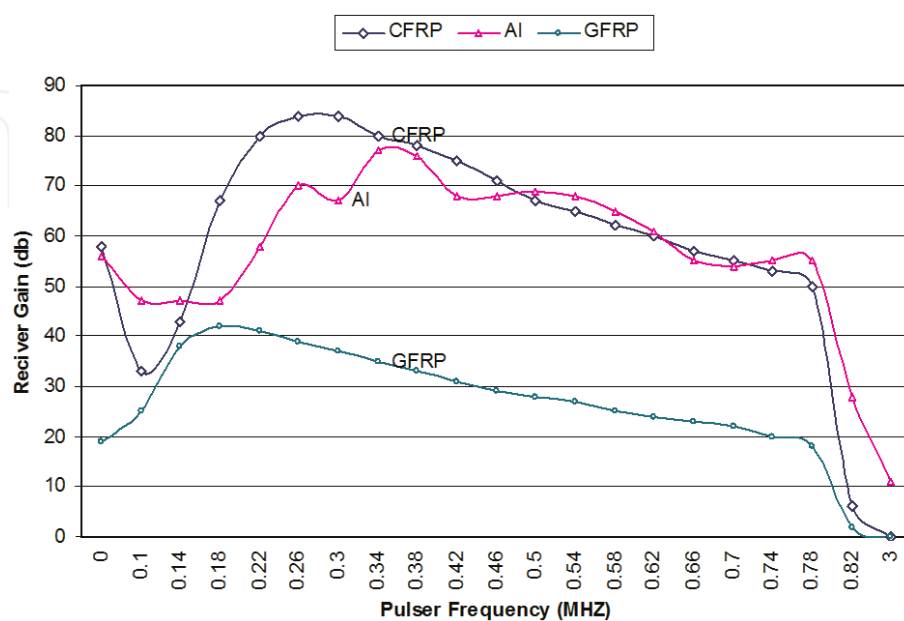


Figure 3.
Optimal driving frequency selection for different materials.

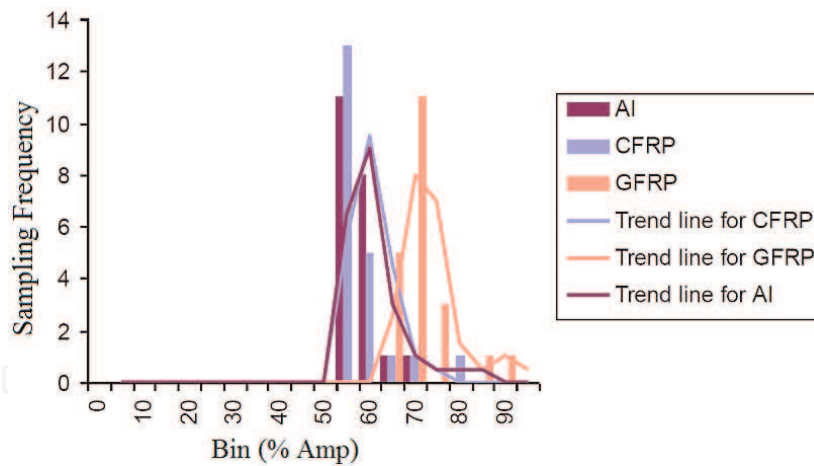


Figure 4.
 Histogram representation of % amplitude of waveform at constant gain.

Material	V_T (m/s)	V_L (m/s)	ν_{12}	E_1 (Gpa)	E_2 (Gpa)	ν_{21}	Density (ρ) kg/m ³
GFRP	6439	3128	0.346	47.31	11.26	0.081	1853
CFRP	8745	4628	0.307	77.74	21.73	0.086	1400

Table 2.
 Material properties arrived from experimental setup.

$$E_1 = \frac{V_T^2 \rho (1 + \nu_{12})(1 - 2\nu_{12})}{1 - \nu_{12}} \quad (1)$$

$$E_2 = \frac{V_L^2 \rho (1 + \nu_{21})(1 - 2\nu_{21})}{1 - \nu_{21}}$$

where V_L is longitudinal velocity of AE and V_T is transverse velocity of AE traveling in the material respectively, ρ is material density and ν_{12} is Poisson's ratio. The material properties of specimens arrived from the experimental setup is presented in **Table 2**.

3. Methodology

In this work a hybrid method has been proposed for identify change in damping capacity of a material using combined finite element and Lamb wave method. The process diagram of the hybrid method for the dynamic mechanical analysis is shown in **Figure 5**.

The group velocity (c_{g_n}), modal frequency (f_n) are determined from Lamb wave model and loss less finite element model respectively.

3.1 Lamb wave model for laminated composite plate

Lamb waves can be of two groups, symmetric and anti-symmetric, these waves propagate independently of the other and boundary conditions of the wave equation are being satisfied by both of them for this problem. Actuating frequency relating the velocity of Lamb wave propagation has been derived in the following section. Dispersion curves of Lamb wave in a particular material, which plot the

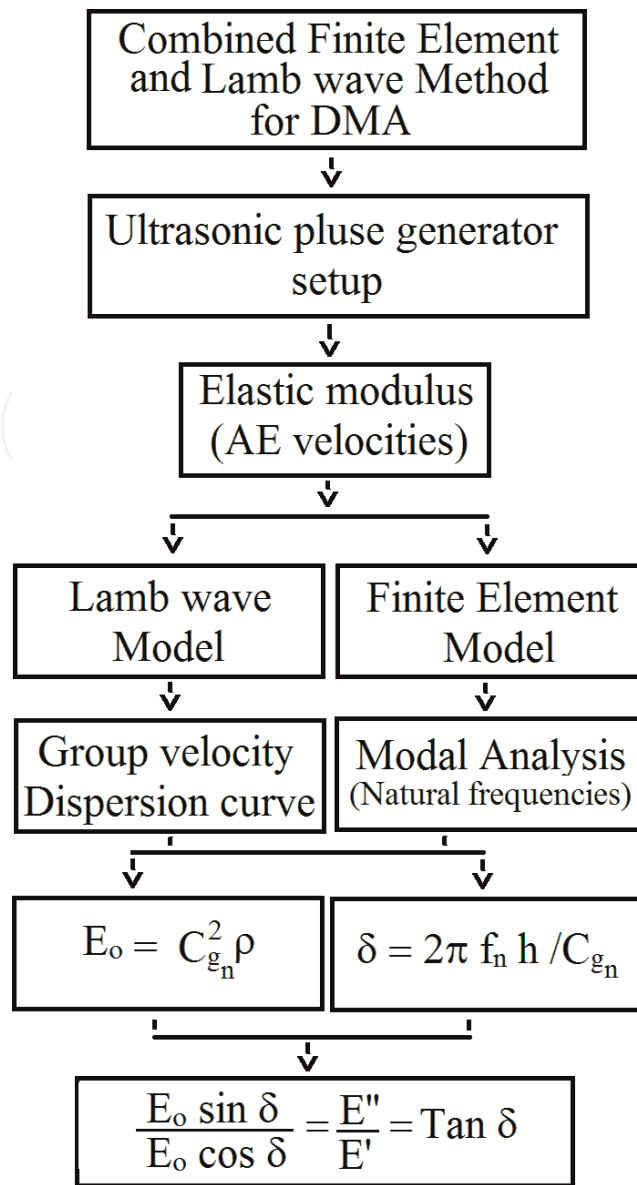


Figure 5. Methodology chart for dynamic mechanical analysis by hybrid method.

phase and group velocities versus the excitation frequency given by Dalton et al. [24]. The anti-symmetric Lamb wave solution formulated as seen in Eq. 2:

$$\frac{\tan(qh)}{\tan(ph)} = \frac{(k^2 + q^2)^2}{4k^2qp} \quad (2)$$

where $p^2 = \frac{\omega^2}{c_l^2} - k^2$, $q^2 = \frac{\omega^2}{c_t^2} - k^2$, and $k = \frac{\omega}{c_{phase}}$

individual laminate stress-strain relationship is given by

$$\begin{bmatrix} \sigma_1 \\ \sigma_2 \\ \tau_6 \end{bmatrix} = \begin{bmatrix} Q_{11} & Q_{12} & 0 \\ Q_{12} & Q_{22} & 0 \\ 0 & 0 & Q_{66} \end{bmatrix} \begin{bmatrix} \varepsilon_1 \\ \varepsilon_2 \\ \gamma_6 \end{bmatrix} \quad (3)$$

where σ is normal stress, τ represent shear stress, ε is normal strain and γ represent the shear strain. Reduced stiffness components Q_{ij} are defined in terms of the engineering constants as

$$\begin{aligned} Q_{11} &= E_1/(1 - \nu_{12}\nu_{21}) \\ Q_{22} &= E_2/(1 - \nu_{12}\nu_{21}) \\ Q_{12} &= \nu_{12}E_1/(1 - \nu_{12}\nu_{21}) \end{aligned} \quad (4)$$

where E_1 Young's moduli in the longitudinal and E_2 Young's moduli in the transverse directions. The major and minor Poisson's ratios represented by ν_{12} and ν_{21} respectively. The relation between Poisson's ratios in Eq. (4) is given by:

$$\nu_{21} = \frac{E_2}{E_1} \nu_{12} \quad (5)$$

A_{11} and A_{22} , are in-plane stiffnesses of plate and these are obtained by integrating the Q_{ij} across the thickness of the plate [21]. These stiffness values are given as:

$$A_{ij} = \int_{-h/2}^{h/2} (Q'_{ij})_k dz, \quad i, j = 1, 2, \quad (6)$$

where plate thickness is represented by "h" and "k" represents each individual lamina. The transformed stiffness coefficients Q'_{ij} are defined as

$$\begin{aligned} Q'_{11} &= m^4 Q_{11} + n^4 Q_{22} + 2m^2 n^2 Q_{12} + 4m^2 n^2 Q_{66} \\ Q'_{22} &= n^4 Q_{11} + m^4 Q_{22} + 2m^2 n^2 Q_{12} + 4m^2 n^2 Q_{66} \\ Q'_{12} &= m^2 n^2 Q_{11} + m^2 n^2 Q_{22} + (m^4 + n^4) Q_{12} - 4m^2 n^2 Q_{66} \end{aligned} \quad (7)$$

where $m = \cos(\theta)$ and $n = \sin(\theta)$, the angle θ is taken positive for counterclockwise rotation and it is considered from the primed (laminated) axes to the unprimed (individual lamina) axes. Q'_{ij} for the 0° and 90° laminas are given by

$$\begin{aligned} (Q'_{11})_{0 \text{ deg}} &= Q_{11} \quad (Q'_{11})_{90 \text{ deg}} = Q_{22} \\ (Q'_{22})_{0 \text{ deg}} &= Q_{22} \quad (Q'_{22})_{90 \text{ deg}} = Q_{11} \\ (Q'_{12})_{0 \text{ deg}} &= Q_{12} \quad (Q'_{12})_{90 \text{ deg}} = Q_{12} \end{aligned} \quad (8)$$

The extensional plate mode velocity is related to the in-plane stiffness of a composite [14]. A_{11} and A_{22} are the stiffnesses propagating in the 0° and 90° directions respectively. The relation between extensional plate mode velocity and stiffness is given by:

$$\text{for } 0^\circ \text{ direction } c_t = \sqrt{A_{11}/\rho h} \quad (9)$$

$$\text{for } 90^\circ \text{ direction } c_l = \sqrt{A_{22}/\rho h} \quad (10)$$

The inplane stiffnesses A_{11} and A_{22} are calculated using Eqs. (4)–(8) by substituting engineering stiffnesses of the composite. The extensional plate mode velocities are substituted into Eq. (2) and it is solved numerically for phase velocity in MathematicaTH. Phase velocity (c_{phase}) is the dependent variable being solved for the independent variable being iteratively supplied is the frequency-thickness product, where ω is the driving frequency in radians. Group velocity dispersion curve, which are derived from the phase velocity curve using Eq. (11):

$$c_{group} = c_{phase} + \frac{\partial c_{phase}}{\partial k} k = \frac{c_{phase}}{1 - \frac{f}{c_{phase}} \cdot \frac{\partial c_{phase}}{\partial f}} \quad (11)$$

where f is the frequency in Hz.

3.2 Finite element model for free vibration of a laminated composite plate

Natural frequency is the phenomenon that occurs with oscillatory motion at certain frequencies known as characteristic values, and it follows well defined deformation pattern known as mode shapes or characteristic modes. The study free vibration is important in finding the dynamic response of elastic structures. It is assumed that the external force vector \vec{P} to be zero and the harmonic displacement as:

$$\vec{Q} = \underline{\vec{Q}} \cdot e^{i\omega t} \quad (12)$$

and the free vibration is given by:

$$[[k] - \omega^2[M]] \underline{\vec{Q}} = \vec{0} \quad (13)$$

where $\underline{\vec{Q}}$ is displacement amplitude, \vec{Q} eigen vector and ω denotes the natural frequency of vibration. Eq. (12) is a linear algebraic eigenvalue problem where neither $[k]$ nor $[M]$ is a function of the circular frequency (ω), $\underline{\vec{Q}}$ is nonzero solution therefore the determinant of coefficient matrix $[k] - \omega^2[M]$ is zero, i.e.,

$$[k] - \omega^2[M] = 0 \quad (14)$$

where $[k]$ is stiffness matrix and $[M]$ is mass matrix, which are derived through finite element formulation.

Figure 6 shows the plate bending formulation where $x, y,$ and z describes the global coordinate of the plate whereas $u, v,$ and w are the displacements, h represents plate thickness. The xy plane is parallel to the midsurface plane prior to deflection. The displacements in the plate at any point is expressed as

$$u = u(x, y, z) \quad (15)$$

$$v = v(x, y, z) \quad (16)$$

$$w = w(x, y, z) \quad (17)$$

The plane displacement u and v vary through the plate thickness as well as with in the xy -plane while the transverse displacement w remains constant through the plate thickness.

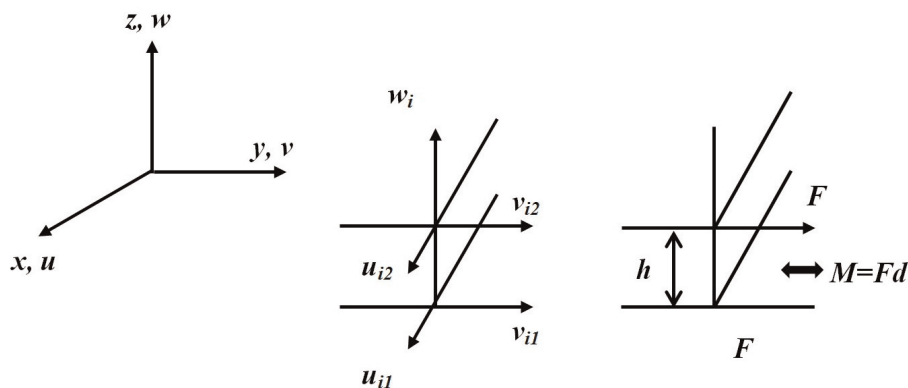


Figure 6.
Plate element with displacement degrees of freedom.

In order to develop shape functions two different interpolations are used one interpolation within the xy -plane and the other in the z -axis. For the xy -plane interpolation, shape function $N_i(x,y)$ are used where subscript i varies depending on the number of nodes on the xy -plane. Shape function $H_j(z)$ is used for interpolation along the z -axis, where subscript j varies depending on the number of nodes along the plate thickness. Since two inplane displacement are functions of x , y , and z , both shape functions are used while the shape functions $N_i(x,y)$ was used for transverse displacement. The mapping of ξ, η -plane onto xy -plane and ζ -axis to z -axis, was done using isoparametric element and the three displacements are expressed as

$$u = \sum_{i=1}^{N_1} \sum_{j=1}^{N_2} N_i(\xi, \eta) H_j(\zeta) u_{ij} \quad (18)$$

$$v = \sum_{i=1}^{N_1} \sum_{j=1}^{N_2} N_i(\xi, \eta) H_j(\zeta) v_{ij} \quad (19)$$

$$w = \sum_{i=1}^{N_1} N_i(\xi, \eta) w_i \quad (20)$$

where N_1 represents the number of nodes in xy -plane (ξ, η -plane) and N_2 represents the number of nodes in z -axis (ζ -axis). The first subscript for u and v denotes the node numbering in terms of xy -plane (ξ, η -plane) and the second subscript indicates the node numbering in terms of z -axis (ζ -axis). Four-node quadrilateral shape function is considered for the xy -plane (ξ, η -plane) interpolation, i.e., $N_1 = 4$ and $N_2 = 2$ that is linear shape function which is considered for the z -axis (ζ -axis) interpolation. Nodal displacement u_{i1} and v_{i1} are displacement on the bottom surface of the plate element and u_{i2} and v_{i2} are displacement on the top surface. As seen in Eqs. (18)–(20), there is no rotational degree of freedom for the present plate bending element were as both bending strain energy and transverse shear strain energy are included.

The relation between bending strains and transverse shear strain with respect to displacements is given by:

$$\{\varepsilon_b\} = \begin{Bmatrix} \varepsilon_x \\ \varepsilon_y \\ \gamma_{xy} \end{Bmatrix} = \begin{bmatrix} \frac{\partial}{\partial x} & 0 & 0 \\ 0 & \frac{\partial}{\partial y} & 0 \\ \frac{\partial}{\partial y} & \frac{\partial}{\partial x} & 0 \end{bmatrix} \begin{Bmatrix} u \\ v \\ w \end{Bmatrix} \quad (21)$$

$$\{\varepsilon_s\} = \begin{Bmatrix} \gamma_{yz} \\ \gamma_{xz} \end{Bmatrix} = \begin{bmatrix} \frac{\partial}{\partial z} & 0 & \frac{\partial}{\partial x} \\ 0 & \frac{\partial}{\partial z} & \frac{\partial}{\partial y} \end{bmatrix} \begin{Bmatrix} u \\ v \\ w \end{Bmatrix} \quad (22)$$

where $\{\varepsilon_b\}$ and $\{\varepsilon_s\}$ are the bending strain and transverse shear strain respectively. The normal strain along the plate thickness ε_z is not considered.

Substitution of Eqs. (18)–(20), into the Eqs. (25) and (26), with $N_1 = 4$ and $N_2 = 2$ gives:

$$\{\varepsilon_s\} = [B_b] \{d^e\} \quad (23)$$

where

$$[B_b] = [[B_{b1}] [B_{b2}] [B_{b3}] [B_{b4}]] \quad (24)$$

$$[B_b] = \begin{bmatrix} H_1 \frac{\partial N_i}{\partial x} & 0 & H_2 \frac{\partial N_i}{\partial x} & 0 & 0 \\ 0 & H_1 \frac{\partial N_i}{\partial y} & 0 & H_2 \frac{\partial N_i}{\partial y} & 0 \\ H_1 \frac{\partial N_i}{\partial y} & H_1 \frac{\partial N_i}{\partial x} & H_2 \frac{\partial N_i}{\partial y} & H_2 \frac{\partial N_i}{\partial x} & 0 \end{bmatrix} \quad (25)$$

$$\{d^e\} = \{ \{d_1^e\} \quad \{d_2^e\} \quad \{d_1^e\} \quad \{d_2^e\} \}^T \quad (26)$$

$$\{d_i^e\} = \{ u_{i1} \quad v_{i1} \quad u_{i2} \quad v_{i2} \quad w_i \} \quad (27)$$

$$\{\varepsilon_s\} = [B_s]\{d^e\} \quad (28)$$

where

$$[B_s] = [[B_{s1}] [B_{s2}] [B_{s3}] [B_{s4}]] \quad (29)$$

$$[B_{si}] = \begin{bmatrix} N_i \frac{\partial H_1}{\partial z} & 0 & N_i \frac{\partial H_2}{\partial z} & 0 & \frac{\partial N_i}{\partial x} \\ 0 & N_i \frac{\partial H_1}{\partial z} & 0 & N_i \frac{\partial H_2}{\partial z} & \frac{\partial H_2}{\partial y} \end{bmatrix} \quad (30)$$

The constitutive equation is

$$\{\sigma_b\} = [D_b]\{\varepsilon_b\} \quad (31)$$

$$\{\sigma_b\} = \{ \sigma_x \quad \sigma_y \quad \tau_{xy} \}^T \quad (32)$$

$$[D_b] = \frac{E}{1-\nu^2} \begin{bmatrix} 1 & \nu & 0 \\ \nu & 1 & 0 \\ 0 & 0 & \frac{1-\nu}{2} \end{bmatrix} \quad (33)$$

For the bending components

$$\{\sigma_s\} = [D_s]\{\varepsilon_s\} \quad (34)$$

where

$$\{\sigma_s\} = \{ \tau_{yz} \quad \tau_{xz} \}^T \quad (35)$$

$$[D_s] = \frac{E}{2(1+\nu)} \begin{bmatrix} 1 & 0 \\ 0 & 1 \end{bmatrix} \quad (36)$$

where Eq. (33) is for the plane stress condition for the plate bending theory and for a FRP composite, is given by

$$[D_b] = \begin{bmatrix} D_{11} & D_{12} & 0 \\ D_{12} & D_{22} & 0 \\ 0 & 0 & D_{33} \end{bmatrix} \quad (37)$$

In which

$$D_{11} = \frac{E_1}{1 - \nu_{12}\nu_{21}} \quad (38)$$

$$D_{12} = \frac{E_1\nu_{21}}{1 - \nu_{12}\nu_{21}} \quad (39)$$

$$D_{22} = \frac{E_2}{1 - \nu_{12}\nu_{21}} \quad (40)$$

$$D_{33} = G_{12} \quad (41)$$

And

$$[D_s] = \begin{bmatrix} G_{13} & 0 \\ 0 & G_{12} \end{bmatrix} \quad (42)$$

Here, the longitudinal direction is represented with 1 and transverse direction is represented with 2 for the FRP composite. Further E_i and G_{ij} are the elastic modulus and shear modulus respectively, whereas ν_{ij} is Poisson's ratio for strain in the j -direction. Five independent material properties will be considered for Eqs. (37)–(42) because of the reciprocal relation

$$\frac{\nu_{12}}{E_1} = \frac{\nu_{21}}{E_2} \quad (43)$$

The stiffness matrix of the element $[k^{(e)}]$ is expressed as:

$$[k^{(e)}] = \int_{\Omega^e} [B_b]^T [D_b] [B_b] \partial\Omega + \int_{\Omega^e} [B_s]^T [D_s] [B_s] \partial\Omega \quad (44)$$

where Ω represents the plate domain. Similarly the mass matrix is given by

$$[M^{(e)}] = \frac{\rho A t}{9} \begin{bmatrix} 4 & 2 & 1 & 2 \\ 2 & 4 & 2 & 1 \\ 1 & 2 & 4 & 2 \\ 2 & 1 & 2 & 4 \end{bmatrix} \quad (45)$$

where A is area of the element, t is the element thickness and ρ density of material. Natural frequencies are arrived for composite plates from the lossless finite element formulation. The MathematicaTH software has been used to compute the Eigen values using the inputs taken from the experimental data discussed in the previous sections. The analytical model developed was correlated ANSYS model. Block Lanczos method was used to carry out modal analysis in ANSYS. The analysis was done for 30 subsets and shell-190 has been used as meshing element. **Figures 7** and **8** shows the first and twentieth mode of natural frequency of the undamaged specimen, i.e., GFRP and CFRP respectively and similarly **Figures 9** and **10** shows for damaged specimen.

3.3 Bandwidth method

The damping parameters in FRP composites are based on the energy dissipation mechanism. Vibrational parameters such as frequency and amplitude are used to

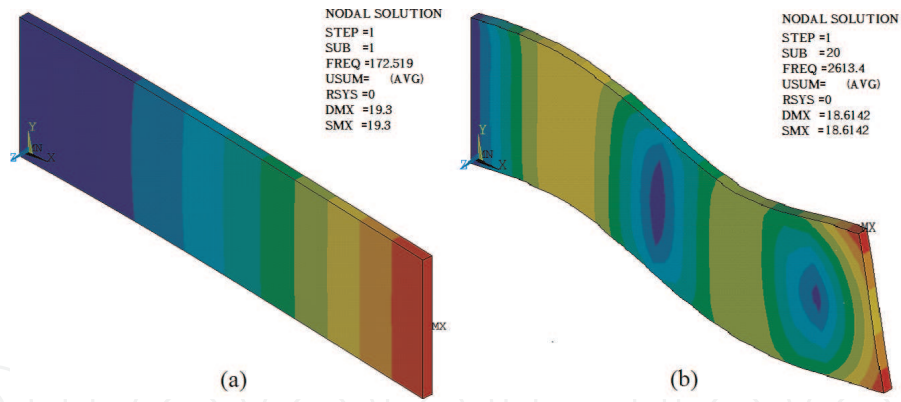


Figure 7. Undamaged GFRP specimen's first and twentieth mode of natural frequency.

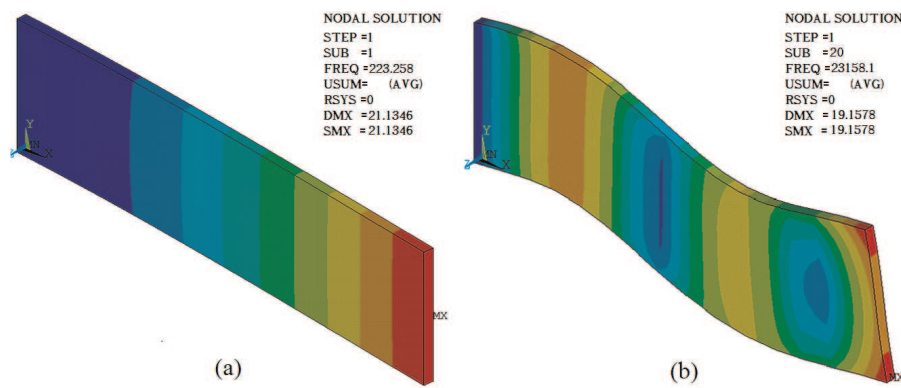


Figure 8. Undamaged CFRP specimen's first and twentieth mode of natural frequency.

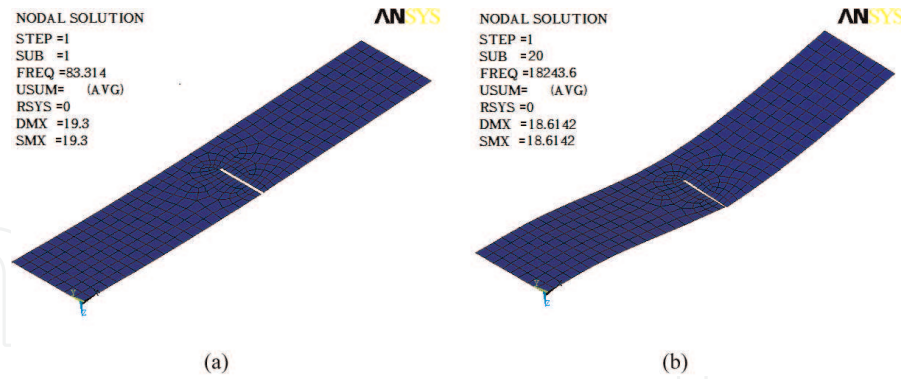


Figure 9. Damaged GFRP specimen's first and twentieth mode of natural frequency.

determine the dynamic characteristics of a system. The best practice to study vibrational parameters is with nondestructive evaluation. Damping characteristics of a system can be determined by the maximum response, i.e., the response at the resonance frequency as indicated by the maximum value of R_p . **Figure 11** illustrates the Bandwidth method of damping measurement where, damping in a system is indicated by the sharpness or width of the response curve in the vicinity of a resonance frequency ω_r , designating the width as a frequency increment (i.e., $\Delta\omega = \Delta\omega_2 - \omega_1$) measured at the “half-power point” (i.e., at a value $(R/\sqrt{2})$) and the damping ratio ζ can be estimated by using band width in the relation given by

$$\zeta = \frac{\Delta\omega}{2\omega_r} \quad (46)$$

for i^{th} mode damping ratio is given by

$$\zeta_i = \frac{1}{2} \frac{\Delta\omega_i}{\omega_i} \quad (47)$$

The equation of motion of a system with viscous damping, when the excitation is a force $F = F_o \sin \omega t$ applied to the system, is given by

$$m\ddot{x} + c\dot{x} + kx = F_o \sin \omega t \quad (48)$$

Eq. (48) represents the forced vibration of a damped system and the resulting motion occurs at the forcing frequency ω . The damping coefficient c is greater than zero, leads to change in the phase between the force and resulting motion. The phase change is termed as phase angle δ which is a function of the frequency ratio ω/ω_r and for several values of the fraction of critical damping ζ , given by [25].

$$\delta = \tan^{-1} \frac{2\zeta(\omega/\omega_r)^3}{1 - (\omega^2/\omega_r^2) + (2\zeta\omega/\omega_r)^2} \quad (49)$$

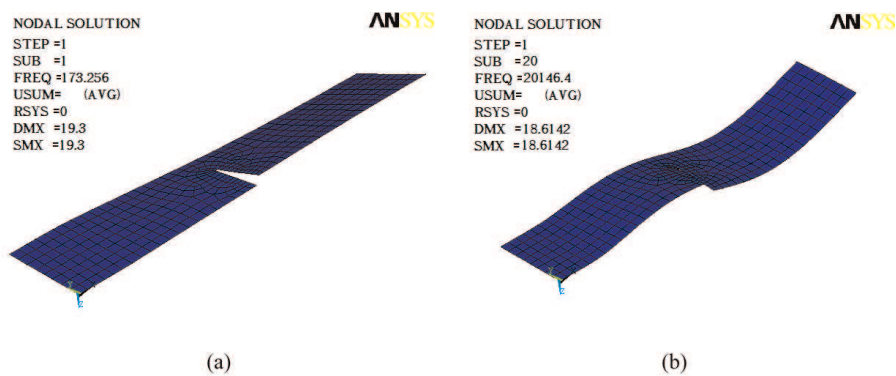


Figure 10.
 Damaged CFRP specimen's first and twentieth mode of natural frequency.

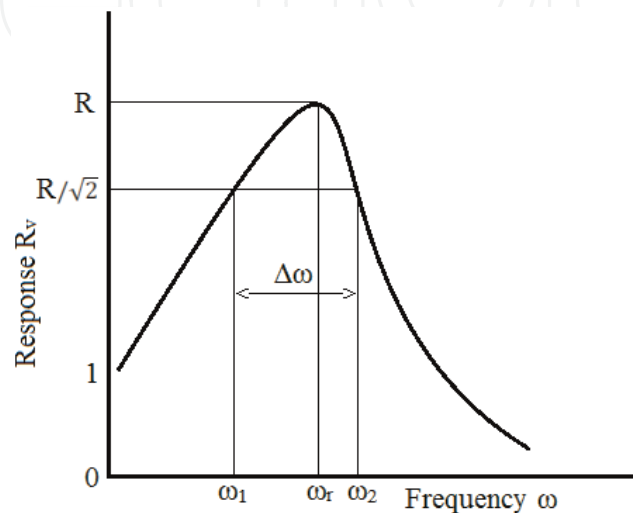


Figure 11.
 Response curve showing bandwidth at half-power point.

4. Results and discussion

The phenomenon of change in modal parameters has been used to identify the damage in the specimens. The damage in the specimen is identified by change in damping capacity with respect to undamaged specimen. The first order Lamb wave equation is used to determine the storage modulus. Lamb wave propagating is quite complex to understand, i.e., an increase in modulus slightly speeds the wave velocity. An increase in the density would have the opposite effect slowing wave velocity, as it appears in all the same terms as the modulus but on the reciprocal side of the divisor.

The AE velocities of the specimens were arrived experimentally using ultrasonic pulse generator test setup and the engineering constants, Young's modulus and poisson's ratio were calculated. The engineering constants are substituted in Lamb wave model discussed in previous sections for finding dispersion characteristics shown in **Figure 12**. The same material properties are used for finite element model to determine natural frequencies.

The group velocity (c_{g_n}) at natural frequency (f_n) and thickness (h) is substituted in Eq. (50) to determine the phase shift and thus finding material damping capacity ($Tan \delta$). Dynamic mechanical analysis can be carried out using the same procedure by getting the E_o value from group velocity dispersion at iteratively supplied frequencies.

$$\delta = 2\pi f_n h / c_{g_n} \quad (50)$$

$$E_o = c_{g_n}^2 \cdot \rho \quad (51)$$

Damping is the term used in vibration and noise analysis to describe any mechanism whereby mechanical energy in the system is dissipated. The damping properties of so-called damping materials, such as elastomeric materials, are usually temperature and frequency dependent, so the experimental determination of damping material properties requires a long and repeating process.

In dynamic mechanical analysis damping measurements is done in temperature sweep mode whereas in this work frequency sweep mode is used. In the present work damping measurements were carried out using combined finite element and Lamb wave method and the results were compared with bandwidth method.

The modal analysis was carried out using developed finite element model and it was correlated with ANSYS. The waveform from the instrument is processed through virtual controlling software and the continuous waveform is subjected to

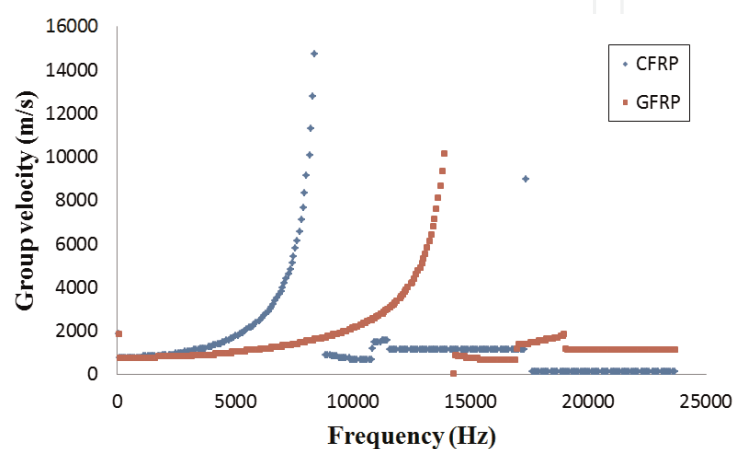


Figure 12.
Lamb wave dispersion curves of CFRP and GFRP.

fast Fourier transform (FFT) which yield a single peak from the calibrated optimal driving frequency, however for a few finite cycles, the FFT appears as a Gaussian curve. The response curve of the undamaged and damaged specimens being tested for damping capacity using bandwidth method is shown in **Figure 13**.

The Lamb wave dispersion curves have been obtained from the iterative supply of the frequency using MathematicaTH code. The group velocity dispersion curve of the specimens used in this research is shown in **Figure 12**. The group velocities and the natural frequencies obtained from modal analysis are used to determine damping capacity at various mode of interest.

Table 3 shows the damping capacities of the undamaged specimen in comparison at critical modes similarly for damaged specimen it has been reported in **Table 4**. It is observed that the natural frequencies of the damaged specimen fell down and the damping capacities have increased slightly with respect to undamaged specimens. **Figure 14** shows the damping capacities and dynamic

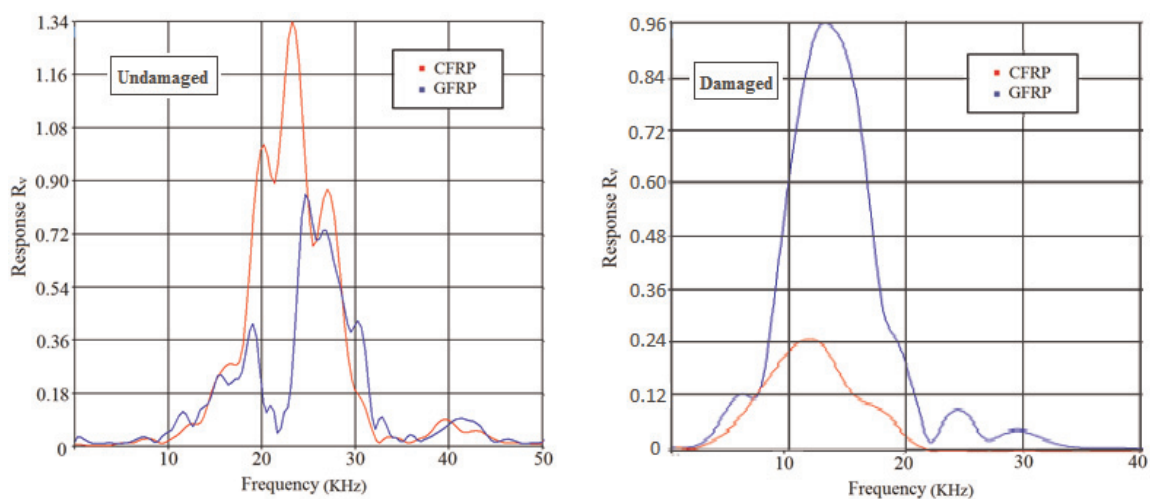


Figure 13.
 Response curve of GFRP and CFRP showing bandwidth.

Material	Natural frequency (Hz)	Lamb wave method (Damping capacity)	Mode frequency(Hz)	Bandwidth method (Damping capacity)
GFRP	172(1 st)	0.0000493	8692	0.001394
	9970(10 th)	0.0012204	11537	0.002427
	21606(20 th)	0.0043671	19248	0.004251
CFRP	223(1 st)	0.0000646	8706	0.004569
	11023(10 th)	0.0016254	20835	0.021765
	23158(20 th)	0.0516527	23164	0.049638

Table 3.
 Damping capacity of undamaged test specimens.

Material	Natural frequency (Hz)	Lamb wave method (Damping capacity)	Mode frequency(Hz)	Bandwidth method (Damping capacity)
GFRP	83.314(1 st)	0.0001542	3692	0.001632
	5216.32(10 th)	0.0021472	6924	0.002951
	18243.6(20 th)	0.0048795	14248	0.004793
CFRP	173.256(1 st)	0.00013258	4733	0.005042
	9872.93(10 th)	0.0023742	12841	0.02635
	20146.4(20 th)	0.057483	11457	0.05539

Table 4.
 Damping capacity of damaged test specimens.

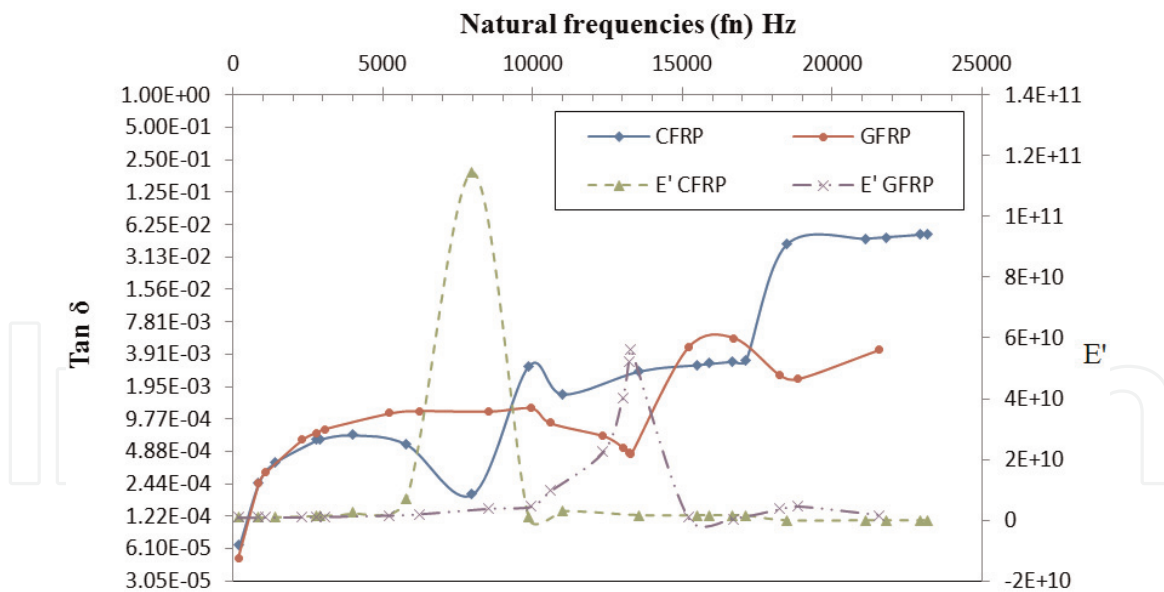


Figure 14.
Damping capacity and dynamic storage modulus for CFRP and GFRP.

storage modulus of the tested specimens with respect to their natural frequencies. The material GFRP and CFRP exhibits similar damping property to a certain range of frequency, and in between 2 and 8 kHz GFRP has better damping property among the two and at higher range of frequencies CFRP is found to be good in damping characteristics.

5. Conclusions

Dynamic mechanical analysis is a technique used to study and characterize damping behavior of materials. It is most useful for studying the viscoelastic behavior of polymers. The tests were conducted on polymer composites CFRP and GFRP laminates in their undamaged and damaged state. A hybrid method has been explored in this work and the materials have been characterized for damping parameters at their mode frequencies. The change in the modal parameters (i.e., natural frequencies and damping capacity) can be used to identify and assesses the health of the structures. It is very advantageous method to obtain damping characteristics of the materials at higher frequency and at relatively low amplitudes.

IntechOpen

IntechOpen

Author details

Beera Satish Ben^{1*} and Beera Avinash Ben²

1 National Institute of Technology, Warangal, India

2 Avanthi Institute of Engineering and Technology, Visakhapatnam, India

*Address all correspondence to: satishben@nitw.ac.in

IntechOpen

© 2019 The Author(s). Licensee IntechOpen. This chapter is distributed under the terms of the Creative Commons Attribution License (<http://creativecommons.org/licenses/by/3.0>), which permits unrestricted use, distribution, and reproduction in any medium, provided the original work is properly cited. 

References

- [1] Doebling S, Farrar C, Prime M, Shevits D. Damage Identification and Health Monitoring of Structural and Mechanical Systems from Changes in Their Vibration Characteristics: A Literature Review. USA: Los Alamos National Laboratory; 1996. pp. 1-136
- [2] Lifshitz J, Rotem A. Determination of reinforcement unbonding of composites by a vibration technique. *Journal of Composite Materials*. 1969;**3**:412-423
- [3] Das S, Saha P, Patro SK. Vibration-based damage detection techniques used for health monitoring of structures. A review. *Journal of Civil Structural Health Monitoring*. 2016;**6**:477-507
- [4] Gillich GR, Praisach ZI. Modal identification and damage detection in beam-like structures using the power spectrum and time-frequency analysis. *Signal Processing*. 2014;**96**:29-44
- [5] Kyriazoglou C, Guild FJ. Finite element prediction of damping of composite GFRP and CFRP laminates—A hybrid formulation-vibration damping experiments and Rayleigh damping. *Composites Science and Technology*. 2007;**67**:2643-2654
- [6] Berthelot JM, Sefrani Y. Damping analysis of unidirectional glass and Kevlar fibre composites. *Composites Science and Technology*. 2004;**64**:1261-1278
- [7] Berthelot JM. Damping analysis of orthotropic composites with interleaved viscoelastic layers: Modeling. *Journal of Composite Materials*. 2006;**40**(21):1889-1909
- [8] Berthelot JM, Sefrani Y. Damping analysis of unidirectional glass fiber composites with interleaved viscoelastic layers: Experimental investigation and discussion. *Journal of Composite Materials*. 2006;**40**(21):1911-1932
- [9] Mahi AE, Assarar M, Sefrani Y, Berthelot JM. Damping analysis of orthotropic composite materials and laminates. *Composites Part B Engineering*. 2008;**39**:1069-1076
- [10] Berthelot JM. Damping analysis of laminated beams and plates using the Ritz method. *Composite Structures*. 2006;**74**:186-201
- [11] Berthelot JM, Assarar M, Sefrani Y, Mahi AE. Damping analysis of composite materials and structures. *Composite Structures*. 2008;**85**:189-204
- [12] Chen Y, Gibson RF. Analytical and experimental studies of composite isogrid structures with integral passive damping. *Mechanics of Advanced Materials and Structures*. 2003;**10**(2):127-143
- [13] Montanari L, Basu B, Spagnoli A, Broderick BM. Damage assessment in a cracked fiber-reinforced cantilever beam using Wavelet-Kurtosis techniques. *Key Engineering Materials*. 2013;**569**:1226-1233
- [14] Sharma DS, Munjla MJ, Barad KH. Vibration-based nondestructive technique to detect crack in multi-span beam. *Nondestructive Testing and Evaluation*. 2015;**30**:1-21
- [15] Botelho EC, Pardini LC, Rezende MC. Damping behavior of continuous fiber/metal composite materials by the free vibration method. *Composites Part B Engineering*. 2006;**37**:255-264
- [16] Guan H, Gibson RF. Micromechanical models for damping in woven fabric-reinforced polymer matrix composites. *Journal of*

Composite Materials. 2001;**35**(16):
1417-1434

[17] Mu B, Wu HC, Yan A, Warnemuende K, Fu G, Gibson RF, Kim DW. FEA of complex bridge system with FRP composite deck. *Journal of Composites for Construction*. 2006;**10**(1):79-86

[18] Cao MS, Sha GG, Gao YF, Ostachowicz W. Structural damage identification using damping: A compendium of uses and features. *Smart Materials and Structures*. 2017; **26**(4):043001

[19] Ben BS, Ratnam C, Ben BA, Yang SH. Ultrasonic based method for damage identification in composites materials. *International Journal of Mechanics and Materials in Design*. 2012;**8**:297-309

[20] Ben BS, Ratnam C, Ben BA, Yang SH. Ultrasonic based structural damage detection using combined finite element and model Lamb wave propagation parameters in composite materials. *International Journal of Advanced Manufacturing Technology*. 2013;**67**:1847-1856

[21] Ben BS, Ratnam C, Ben BA, Vikram KA, Yang SH. Damage identification in composite materials using ultrasonic based Lamb wave method. *Measurement*. 2013;**46**: 904-912

[22] Ben BS, Ben BA, Kweon SH, Yang SH. Structural damping of composite materials using combined FE and Lamb wave method. *Structural Engineering and Mechanics*. 2014;**51**:1047-1065

[23] Ratnam C, Ben BS, Ben BA. Structural damage detection using combined finite element and model Lamb wave propagation parameters. *Journal of Mechanical Engineering Science Part C*. 2009;**223**:769-777

[24] Dalton RP, Cawley P, Lowe MJS. The potential of guided waves for monitoring large areas of metallic aircraft fuselage structure. *Journal of Nondestructive Evaluation*. 2001;**20**: 29-46

[25] Blake RE. Basic vibration theory. In: Piersol AG, Paez TL, editors. *Harris' Shock and Vibration Handbook*. 6th ed. New York: Mc-Graw Hill; 2010